

MARS SOIL PROPERTIES FROM PHOBOS ECLIPSE OBSERVATIONS BY INSIGHT HP³ RAD. N.T. Mueller¹, M. Grott¹, S. Piqueux², M. Lemmon³, J. Maki², R. Lorenz⁴, T. Spohn^{1,5}, S.E. Smrekar², J. Knollenberg¹, T.L. Hudson², M. Siegler⁶, A. Spiga⁷, F. Forget⁷, E. Millour⁷, P. Morgan⁸, A. Hagermann⁹, N. Attree⁹, M. Golombek², W.B. Banerdt²

¹German Aerospace Center (DLR), Institute of Planetary Research, Berlin, Germany. ²Jet Propulsion Laboratory, California Institute of Technology, Pasadena, CA, USA. ³Space Science Institute, Boulder, CO, USA. ⁴Hopkins University Applied Physics Lab, Laurel, MD, USA. ⁵International Space Science Institute, Bern, Switzerland. ⁶PSI, SMU Earth Science, Dallas, TX, USA. ⁷Laboratoire de Météorologie Dynamique (LMD/IPSL) Sorbonne Université, Paris, France ⁸Colorado Geological Survey, Golden, CO, USA. ⁹B.E.S., University of Stirling, Stirling, Scotland, UK.

Introduction: The Heat Flow and Physical Properties Package (HP³) includes an infrared radiometer attached to the deck of the InSight lander [1]. The main objective of this instrument subsystem is to constrain the surface thermal boundary condition for the heat flow measurement carried out by the instrumented tether deployed into the subsurface. The heat flow in the subsurface can be affected by seasonal and diurnal temperature variations, by radiation from the lander, its shadow, and the change in surface albedo caused by dust removal during landing and later deposition. The radiometer is measuring daily average temperature as a function of season and recording diurnal temperature curves and shorter period temperature fluctuations, such as eclipses [2], with a sampling rate of up to ~0.5 Hz. The radiometer observes the surface to the NNW of the lander center (Fig.1)

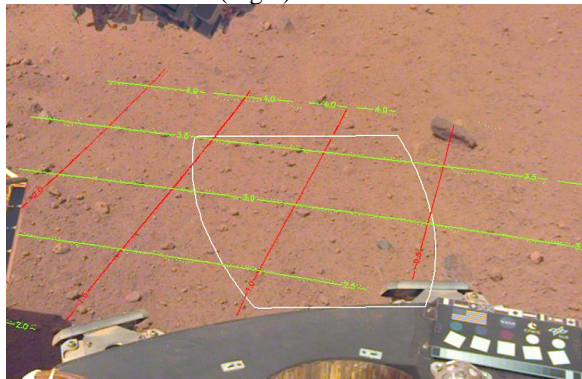


Figure 1: Arm camera image of the surface observed by the radiometer. Green/red lines and labels indicate N/E distance from lander center in m.

Soil properties: The temperature response to changes of insolation provides an estimate of the thermal inertia, which is diagnostic of soil parameters such as grain size and cementation. The HP³ mole encountered soil whose topmost layer is unconsolidated, but has sufficient strength at depth to support a near-vertical wall through the vibrations caused by the hammering mechanism (Fig. 2). Some cementation of the soil at depth is the most likely cause of this unexpected strength.

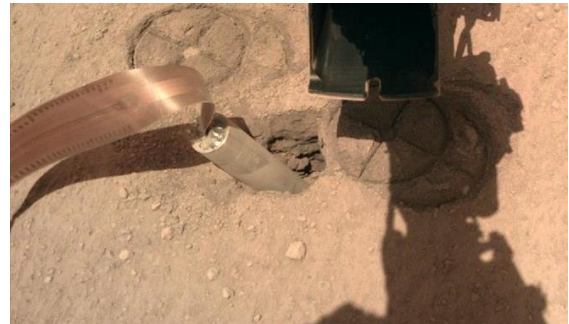


Figure 2: Arm camera image of the hole excavated by the HP³ mole. The mole end is ~5 cm above the surface.

Piqueux et al. [3, this conference] model the diurnal temperature response of the soil observed by the radiometer and find a that the observations can be fitted well assuming a vertically homogeneous soil. The corresponding thermal inertia is $189 \pm 10 \text{ J m}^{-2} \text{ K}^{-1} \text{ s}^{-1/2}$. This value is consistent with orbiter observations of the landing site and has been interpreted as a fine grained sand with an cement volume fraction $\ll 1\%$. Both grain size and cementation increase thermal conductivity of soil and thus thermal inertia [4]. A top layer with different thermal properties, which is thin compared to the diurnal skin depth of a few centimeters, would not strongly affect the diurnal curve, and could therefore be present even though the data is explained well with a homogeneous model. The objective of this research is to find out whether the cementation at depth inferred from images is manifested as a variation of thermal conductivity with depth using data from solar eclipses as an additional constraint.

Eclipse data fitting: On sol 96, 97 and 99 the radiometer observed the effects of Phobos eclipses, which corresponded to a ~30 s long shadow and the reduction of solar flux between 3% and 13%, as observed by the camera and solar panel output. The camera and solar panel data cannot fully resolve the timeline of the insolation reduction and therefore we use a model of that includes Phobos ephemeris, shape and solar limb darkening to generate the timeline. We further use output from the LMD1D model derived from

the MCD model [5] as boundary conditions to solve the heat conduction in the near surface and to calculate model curves of surface temperature. The model accounts for the Mars ephemeris and provides downwelling solar and infrared fluxes. Atmospheric dust opacity is derived from camera images of the sky as used as input for the atmospheric model. At the time of the eclipses the insolation is reduced temporarily according to the eclipse timeline. The free parameters of the model are the thickness of the top layer, the thermal conductivities of both layers and the surface albedo. The model parameters are varied to find the parameter space that provides an acceptable fit to the data, considering its uncertainty.

A challenge in this fit is the weighting of the data. During the eclipse the sampling frequency was set to the maximum of ~ 0.5 Hz while the diurnal curves are typically sampled 23 times in 5 min per solar hour. The radiometer measurement error is dominated by calibration uncertainties, and is expected to be partially a function of local time. That means that the measurement error changes little during the eclipse and therefore does not interfere much with the fit. This is illustrated in Fig. 3. The top panels shows the diurnal curve of sol 97 and the bottom panel focusses on the time around the eclipse sampled at 2 s, with black error bars indicating the total measurement uncertainty. The bottom panel plot indicates that variance relative to the diurnal trends is significantly smaller than that. To make best use of the data we fit them in two steps. First, the diurnal data with the low sampling rate and total uncertainty constrain the parameter space. Second, the high sampling rate data of the eclipse with a smaller uncertainty corresponding to the random noise further narrow down the parameter space. This is work in progress. Fig. 3 shows two models selected to fit within the uncertainty of the data. The blue curve corresponds to homogeneous model with a thermal inertia of $\sim 190 \text{ J m}^{-2} \text{ K}^{-1} \text{ s}^{-1/2}$, and the red curve corresponds to a 5 mm thick top layer with an equivalent thermal inertia of $120 \text{ J m}^{-2} \text{ K}^{-1} \text{ s}^{-1/2}$ above a half-space with properties equivalent to $200 \text{ J m}^{-2} \text{ K}^{-1} \text{ s}^{-1/2}$. Both models fit the amplitude of the diurnal curve but the layer model fits the amplitude of the eclipse response better. The assumption of the total uncertainty underestimates the significance of the latter fit. The thickness of the top layer was here estimated from the images (Fig. 2). although a thinner top layer with a lower thermal inertia equivalent might also fit both diurnal and eclipse response.

Outlook: The combination of observing the mechanical and thermal responses of soil at the InSight landing site provides an opportunity to study the Martian surface in unprecedented detail. This may have an impact on the interpretation of orbiter data as well as

the planning of future mechanical interactions. We expected unconsolidated sand at the landing site and found a material of sufficient strength to inhibit the progress of the HP3 mole via insufficient friction. Possibly a larger than expected fraction of particles smaller than sand (silt) and more cement is to blame. The radiometer data of the diurnal and eclipse indicate some form of layering hinting at this situation, a rigorous exploration of the parameter space consistent with the data is in progress. Laboratory experiments with Mars simulants at Mars pressure illuminated by a solar simulator [e.g. 5] observed by a radiometer might provide some insight whether heterogeneous particulates respond to external forcing changes indicative of the same thermal parameters on both shorter and longer timescales.

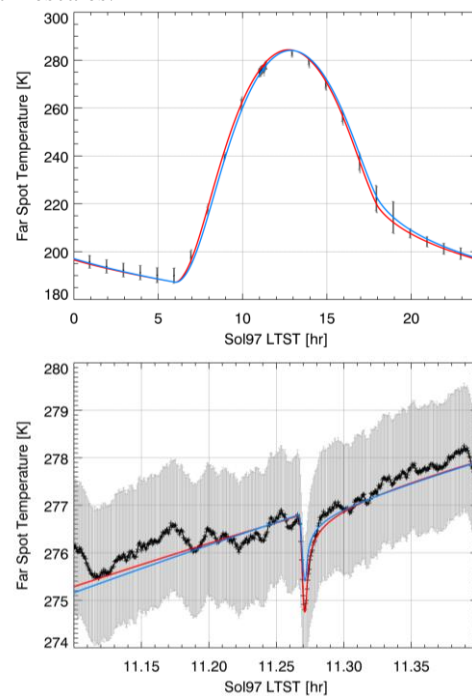


Figure 3: Radiometer data of sol 97. Top: diurnal data, Bottom: eclipse observation. Blue: homogeneous model. Red: layered model. Models described in the text.

References: [1] Spohn, T. et al., *Space Sci. Rev.*, 214:96 (2018). [2] Piqueux, S. & Christensen, P.R. *GRL*, vol.39, L21203, doi:10.1029/2012GL053352, (2012). [3] Piqueux, S. et al. Regolith properties near the InSight lander derived from 100 sols of radiometer measurements. 51st LPSC (2020). [4] Piqueux, S. & Christensen, P.R. *JGR*, vol. 116,E07004, doi:10.1029/2011JE003805, (2011). [5] Millour, E. and the MCD Development Team (2018, Feb). The Mars Climate Database (version 5.3). [6] Kaufmann & Hagermann, *Icarus*, vol. 282, 118-126, doi:10.1016/j.icarus.2016.09.039. (2017)